Materials Advances

ROYAL SOCIETY OF CHEMISTRY

COMMUNICATION

View Article Online
View Journal | View Issue

Cite this: *Mater. Adv.*, 2024, 5, 7601

Received 11th July 2024,
Accepted 2nd September 2024

DOI: 10.1039/d4ma00703d

rsc.li/materials-advances

Porous carbon pellets for physical adsorption of CO_2: size and shape effect†

Baljeet Singh, * Marianna Kemell and Timo Repo *

The continuous rise in atmospheric CO_2 level is a major concern, demanding the development of low-cost, scalable porous sorbents with improved efficiency and recyclability. The current chemical adsorption methods are energy-intensive, creating a demand for low-energy CO_2 capture/removal strategies. Physical adsorption of CO_2 offers an efficient and low-energy alternative. This study explores the design and screening of porous carbon pellets for physical adsorption of CO_2 from 15% CO_2 in N_2 at 30 °C. Various sizes of spherical pellets were designed and investigated for their effect on adsorption capacity and kinetics. Changing the shape from spherical to flakes increased the CO_2 adsorption capacity to 2.2 wt% (0.5 mmol g^{-1}). The pellets were also analysed for cyclic adsorption–desorption to access long-term stability and recyclability, showing approximately 80% selectivity for CO_2 over N_2 over 20 cycles.

Introduction

CO_2 is a major greenhouse gas that significantly contributes to climate change, surpassing 422 ppm in August 2024, an increase of approximately 4 ppm compared to August 2023.[1] Human activities, particularly the burning of fossil fuels for energy, deforestation, and industrial activities, have caused an unprecedented rise in atmospheric CO_2 level, resulting in the emission of 35.8 Gt of CO_2 globally in 2023.[2] The adverse impact of climate change poses a serious threat to our ecosystems, economies, and human health worldwide, making it one of the most pressing challenges of our time. In response, CO_2 capture technologies have emerged as a critical solution for mitigating climate change, focusing on industrial decarbonization, and direct air capture.[3] These technologies are essential for achieving global net zero emissions targets and limiting the temperature rise to 2 °C above pre-industrial levels.[4] Capturing and storing or reusing CO_2 can substantially reduce CO_2 emissions, supporting a smooth transition to renewable energy adsorption and energy efficiency.[4]

As industries shift toward a low-carbon future through industrial decarbonisation, CO_2 capture becomes increasingly vital for sectors that are difficult to decarbonise, such as cement, steel, and chemical production. Sorbents (solids and liquids or both) are an important segment of large-scale deployment of CO_2 capture technologies. An optimised sorbent design ensures a high adsorption capacity, enabling more CO_2 to be captured per unit of sorbent material, thereby reducing the required sorbent quantity and operation costs.[5–9] Well-designed sorbents also minimise energy requirements, lowering overall energy consumption and making the CO_2 capture system more cost-effective. Additionally, the durability of sorbents over multiple capture and regeneration cycles is essential for long-term viability and cost-effectiveness. The adsorption of CO_2 on a solid sorbent involves both physical and chemical interactions, depending on the nature of the support and the type of active sites.[10] Physical adsorption relies on van der Waals forces to attract CO_2 molecules to the sorbent surface, resulting in low heat of adsorption (approximately 10–50 kJ mol^{-1}).[11–13] It is considered a promising low-energy method for efficient CO_2 capture compared to chemical adsorption of CO_2 in amines (approximately 100 kJ mol^{-1}).[14–16]

Porous activated carbon is widely available and offers a large specific surface area and pore volume, making it an ideal material for upscaling into sorbent pellets of various sizes and shapes for CO_2 capture applications.[17] The extensive surface area also facilitates CO_2 adsorption, making it highly effective in capturing CO_2 from industrial emissions. Additionally, porous carbon can be produced from a variety of low-cost precursor materials, such as biomass, and waste carbonaceous products, making it a cost-effective option for large-scale industrial applications, and contributing to a more sustainable and environmental approach. Porous carbon is cheap, easy to produce, and available in large amounts, and has emerged as a

Department of Chemistry, University of Helsinki, FI-00014 Helsinki, Finland.
E-mail: baljeet.singh@helsinki.fi, timo.repo@helsinki.fi

† Electronic supplementary information (ESI) available. See DOI: https://doi.org/10.1039/d4ma00703d

promising material for CO_2 adsorption under a wide range of conditions.[18,19] It is economically more attractive than the other sorbents such as zeolite,[20] MOF,[21–23] silica,[24–29] porous liquid,[30] and other metal oxides.[31] Thereby, porous carbon-based sorbents offer a lower heat of adsorption (10–35 kJ mol^{-1}) compared to MOFs (50 kJ mol^{-1}) and zeolites (30–50 kJ mol^{-1}).[32–35] One of the significant advantages is their relatively low energy requirements for regeneration compared to other sorbents like amine-based materials. Lower energy consumption reduces operational costs and improves the overall efficiency of the CO_2 capture process.

The selection of suitable materials is critical for the economic viability of sorbents, and it must meet certain criteria including high adsorption capacity, high selectivity for CO_2, fast adsorption and desorption kinetics, stability in cycling processes, low cost, and ease of upscaling production.[36–39] Most of these properties can be fine-tuned by designing appropriate materials.[40] However, shaping powder into pellets/monolith/beads can alter the adsorption properties due to reduction of the surface area, pore blockage due to the use of binders, and material degradation from high pressure. Shaping the powder into pellets is more suitable for large-scale deployment due to lower pressure drops, easy transfer, handling, storage, and reusability.[41–44]

Due to the low energy demand to regenerate physically adsorbed CO_2, interest in screening and developing industrial-grade sorbent pellets is continuously increasing.[45] Porous-activated carbon has been explored for the physical adsorption of CO_2; most of the investigations have been conducted using powder.[46–50] The preparation of pellets using activated porous carbon is therefore crucial for commercial applications, with optimisation of the binder-to-powder ratio to minimise the loss of material properties.[51] Several methods have been reported to convert powder into pellets, for example, high palletisation pressure (5000 psi) led to CO_2 adsorption capacity reduction and also increased internal mass transfer resistance compared to the powder.[52] The use of sodium alginate as a binder to shape the powder avoids applying pressure; hence, changes in textural properties can be minimised. On the other hand, alginate is natural, biocompatible, nontoxic, and biodegradable, and the preparation methods employed water, which is non-toxic, so the whole process is environmentally friendly and sustainable.[53] By optimizing sodium alginate and powder ratio, surface area reduction was minimised, and the adsorption properties were maintained. In our recent work, we also prepared silica beads using sodium alginate as a binder, and we observed no reduction in surface area, with PEI functionalized beads showing an average CO_2 capture capacity of 1 mmol g^{-1} for 105 cycles.[54]

Pellets are practical for industrial applications as they need stability in cyclic adsorption–desorption processes and consistent performance under flue gas conditions. Considering these points, we developed pellets using commercially available porous activated carbon (carbon with a specific surface area of 870 m^2 g^{-1} and average pore size of 3.33 nm) and sodium alginate as a binder, known previously for MOF pellet design (generally described as a bead).[55,56] The effect of pellet size and shape was investigated in detail for the physical adsorption of CO_2. All the adsorption analyses were performed using TGA, and 15% CO_2 in N_2 was used to satisfy industrial flue gas conditions. This innovative study introduced a novel approach to optimising CO_2 capture by shaping the powder into various pellet forms, including spherical, cylindrical, hollow cylindrical, and flake shapes. We systematically investigated the impact of pellet size and shape on CO_2 uptake and adsorption kinetics, providing insight into enhancing the efficiency of physical adsorption processes. The smaller sizes and flake shapes significantly improved CO_2 uptake, by demonstrating that the performance of solid sorbent pellets can be enhanced through careful control of pellet size and shapes. This study provides a foundation for developing cost-effective and efficient solid sorbent CO_2 capture technologies. Future work could explore chemical modification to enhance selectivity and adsorption capacity further, making this approach highly viable for industrial applications.

Results and discussion

Although various spherical pellets of different sizes were designed (Fig. S1, ESI†), we chose to analyse only one type of pellet for its morphology and texture properties, as we anticipated that the specific surface area of the other samples would remain unchanged, as the same ratio of powder to binder was used to vary the size and shape. To examine the surface morphology and texture of both the powder and pellet, SEM

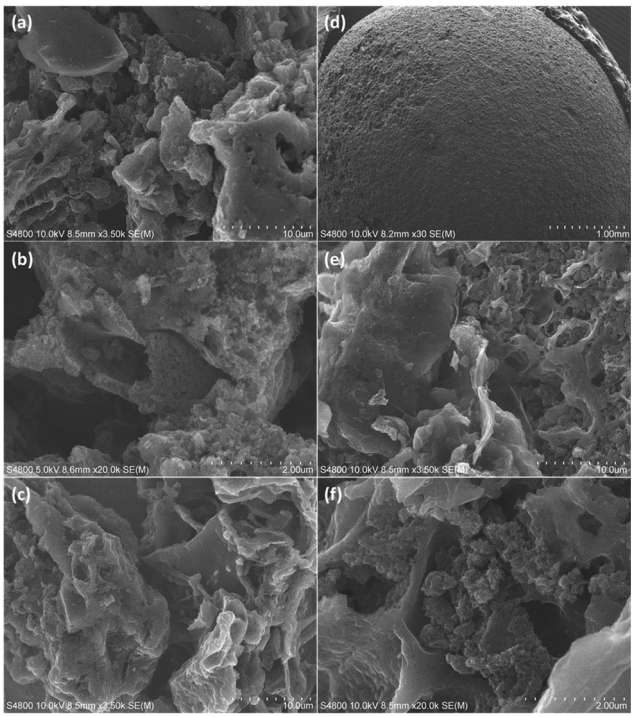

Fig. 1 (a)–(c) SEM images of activated carbon (powder). (d)–(f) SEM image of pellets (P3).

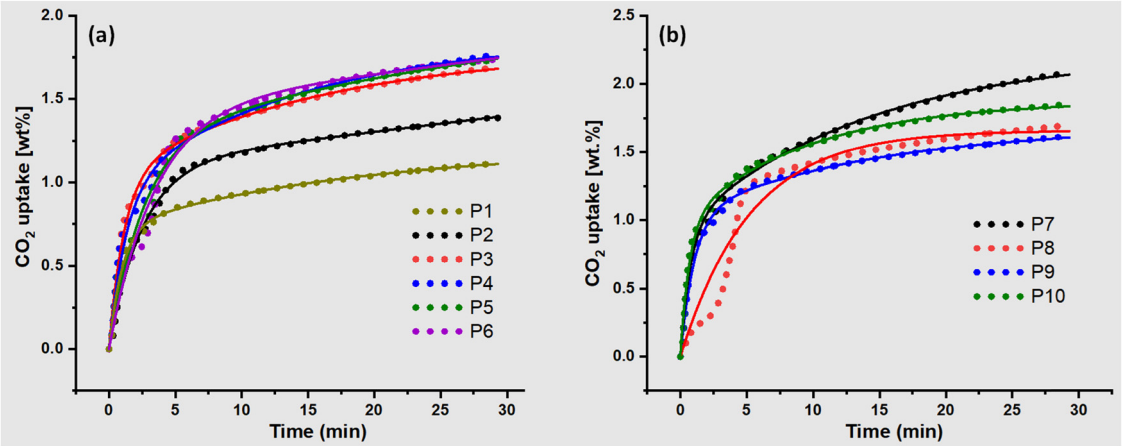

Fig. 2 TGA profiles of adsorption of CO_2; (a) effect of size and (b) effect of shape at 25 °C, 50 ml min^{-1}, 15% CO_2 in N_2. The solid line represents the pseudo-first-order fitting.

Table 1 Fitting parameters of a pseudo-first-order kinetic model for the adsorption of CO_2 over porous carbon pellets

	Size (mm)	Q_{e1}	Q_{e2}	k_1	$k_{1'}$	R^2
P1	4.2	0.72	0.47	0.99	0.055	0.9999
P2	3.7	1.10	—	0.39	—	0.9999
P3	3.3	1.02	0.77	0.87	0.064	0.9999
P4	2.4	0.94	0.92	0.77	0.070	0.9999
P5	1.9	1.24	0.95	0.38	0.025	0.9999
P6	1.8	1.44	—	0.28	—	0.9999
P7	1.2 (T)	0.94	1.29	1.31	0.069	0.9999
P8	4.8 (D)	1.50	0.15	0.19	0.190	0.9999
P9	4.8 (D)	1.03	0.65	0.94	0.069	0.9999
P10	2 (D)	0.98	0.89	1.45	0.105	0.9999

(–) Excluded from the data. T – thickness, D – outer diameter.

analysis was conducted. The SEM images revealed the presence of pores in both the powder (Fig. 1a–c) and pellet (Fig. 1d–f) samples, which could facilitate CO_2 diffusion and promote fast kinetics. N_2 sorption analysis was performed on the P3 pellets (3.3 mm) (Fig. S2, ESI†), revealing a specific surface area of approximately 614 m^2 g^{-1}. This is about 30% lower than the previously reported surface area of the powder sample (876 m^2 g^{-1}). The density functional theory (DFT) pore size distribution of the pellets indicated a narrow range of 0–2 nm, with an average pore size of 1.18 nm (Fig. S3, ESI†), confirming the microporous nature of the pellets.

Effect of size and shape

Six different spherical-size pellets and different shapes (Fig. S1, ESI†) were designed to investigate their effect on CO_2 uptake and kinetics (Fig. S4–S13, ESI†). As the pellet size decreased from P1 to P4, the CO_2 uptake increased from 1.10 wt% to 1.76 wt% (P4, Fig. 2). However, with a further reduction of the pellet to a smaller size than P4, the CO_2 uptake capacity stayed constant. Additionally, changing the shape from spherical to flake (Fig. S14, ESI†), the CO_2 uptake capacity increased to 2.06 wt%, demonstrating the effect of shape and size (Fig. 2b). Although, the solid cylindrical shape (P8) and hollow cylindrical shape (P9) did not show much difference in carbon uptake

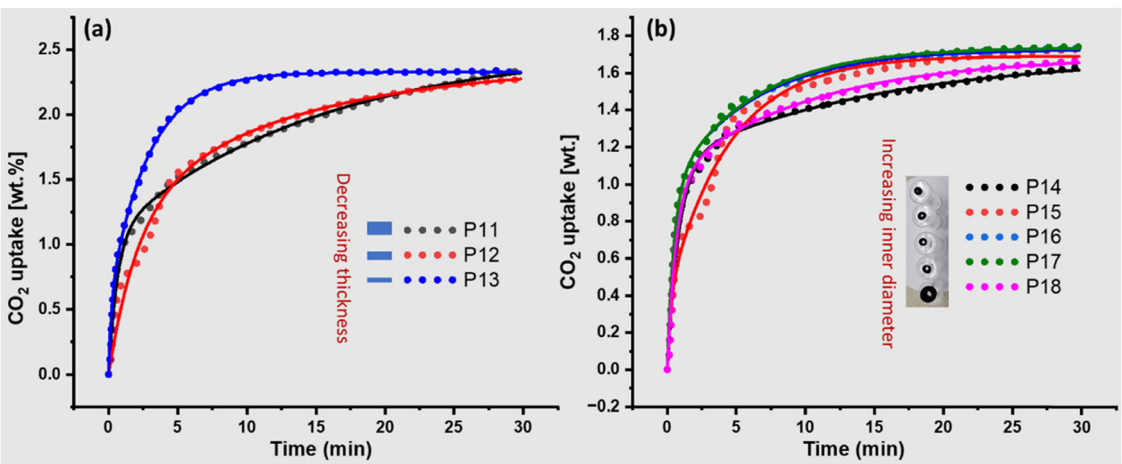

Fig. 3 (a) Effect of thickness of flakes' on the CO_2 adsorption capacity and kinetics. (b) Effect of pellets' inner diameter size (cylindrical) on the adsorption capacity and kinetics.

Table 2 Fitting parameters of a pseudo-first-order kinetic model for the effect of thickness of flakes and inner diameter of hollow pellets

	Size (mm)	Q_{e1}	Q_{e2}	k_1	$k_{1'}$	R^2
P11	1.0 (T)	1.07	1.44	1.57	0.06	0.9999
P12	0.8 (T)	1.23	1.14	0.47	0.08	0.9999
P13	0.3 (T)	0.55	1.77	4.87	0.35	0.9999
P14	4.7 (D)	1.12	0.57	1.18	0.06	0.9999
P15	4.8 (D)	0.38	1.30	3.63	0.22	0.9999
P16	4.7 (D)	0.97	0.75	2.04	0.16	0.9999
P17	4.7 (D)	0.95	0.77	2.07	0.17	0.9999
P18	8.7 (D)	1.02	0.65	1.49	0.10	0.9999
C1	—	0.86	0.83	0.59	2.86	0.9999

C1 – powder sample, T – thickness, D – outer diameter

Table 3 Fitting parameters of a pseudo-first-order kinetic model for the effect of temperature and CO_2 flow rate at constant adsorption temperature

Parameters	Q_{e1}	Q_{e2}	k_1	$k_{1'}$	R^2
Effect of temperature					
30 °C	0.53	2.14	2.80	0.11	0.9999
50 °C	0.51	0.91	2.04	0.19	0.9999
75 °C	0.23	0.48	3.93	0.46	0.9999
Effect of flow					
25 ml min^{-1}	0.26	2.96	5.50	0.08	0.9999
50 ml min^{-1}	0.56	2.01	3.27	0.12	0.9999
75 ml min^{-1}	0.63	1.87	2.88	0.12	0.9999
100 ml min^{-1}	0.64	1.75	2.98	0.12	0.9999

(Fig. S14, ESI†). Notably, reducing the diameter of the solid cylindrical shape pellets increased the CO_2 uptake to 1.8 wt% (P10) compared to 1.68 wt% (P8). The better performance of flakes could be attributed to their more exposed surface area, accessibility of active sites, and better diffusion of CO_2 due to their thickness.

$$Q_t = Q_{e1}(1 - (\exp(-k_1 \cdot t))) + Q_{e2}(1 - (\exp(-k_{1'} \cdot t))) \quad (1)$$

where Q_t is the adsorption capacity in wt% at time t (min). Q_{e1} and Q_{e2} are equilibrium capacities in wt%. k_1 and $k_{1'}$ are the pseudo-first-order rate constant (min^{-1}).

Adsorption kinetics of the pellets

The kinetic modelling of the adsorption curves provides a better understanding of the effect of different sizes and shapes. Typically, a pseudo-first-order model describes physical adsorption; a linear combination of pseudo-first order (eqn (1)) was used to completely fit the TGA CO_2 uptake profiles.[57,58] Instead of dividing the experimental data into two different zones, a single linear combination of pseudo-first-order equations (eqn (1)) was used and found to be most suitable for fitting the experimental data. CO_2 uptake data and corresponding fitting curves for different sizes and shapes of pellets are illustrated in Fig. 1 and relevant kinetic parameters are summarized in Table 1.

Eqn (1) was able to fit the experimental data and the model estimated $Q_t(Q_{e1} + Q_{e2})$ very close to the experimental value. However, in some cases, the model predicted higher values than the experimental data because some of the samples were not saturated in the given time. In that case, we can also consider the overestimated Q_t, which could represent the sample's real equilibrium capacity at the saturation point. As the pellet's size decreased from P1 to P4, the CO_2 uptake increased but it remained constant for P5 and P6, which is also supported by the kinetic parameters. Experimental data showed two adsorption components: initially quick adsorption, likely due to the surface adsorption, followed by a gradual increase in adsorption capacity, which could be due to the slow diffusion of CO_2 in the pores. As the pellet size decreased, Q_{e1} and Q_{e2} increased, indicating that both surface adsorption and inner diffusion improved.

When the shape changed from spherical to flake-type (P7), the CO_2 uptake capacity increased to 2.1 wt%, which was also supported by the kinetic parameters. The rate constant k_1 (1.31) was much higher than any spherical pellets and other shapes, likely due to the increased exposed surface area. As mentioned earlier, Q_{e1} represents fast surface adsorption, while Q_{e2} represents inner pore diffusion of CO_2. The highly exposed surface of the flake's

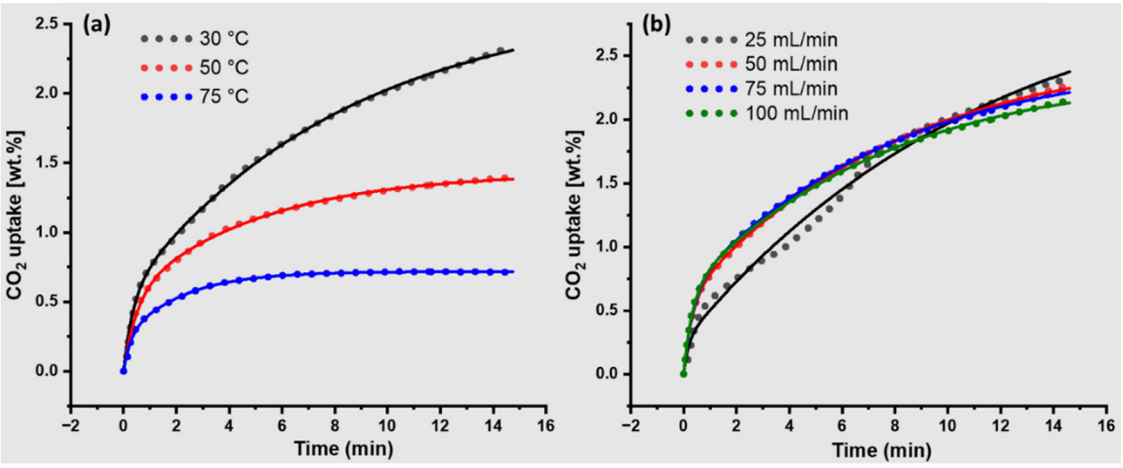

Fig. 4 (a) Effect of adsorption temperature at a fixed CO_2 flow rate of 50 ml min^{-1}. (b) Effect of different flow rates of CO_2 at a fixed adsorption temperature (30 °C).

shape led to much faster saturation than another shape, as supported by the k_1 value (Table 1). Pore diffusion and saturation were also completed at the same time as other spherical and shaped pellets. Q_{e2}, *i.e.*, 1.29 wt%, is the highest among all sizes and shapes, with similar rate constants of k_1 (0.069).

Effect of thickness of the flakes and inner diameter of the hollow cylindrical pellets

We hypothesized that increasing the thickness of the flakes and modifying the pore diameter of the hollow pellets would alter the CO_2 uptake and kinetics (Fig. S14–S22, ESI†). Specifically, we expected a decrease in adsorption capacity and a change in kinetics in both cases. As with decreasing flake thickness, the CO_2 uptake capacity increased to 2.2 wt% and reached saturation (P13) faster compared to P11 and P12, with corresponding changes in kinetics parameters (Fig. 3a and Table 2). The thinnest flake (P13) showed much faster adsorption saturation compared to other flakes (P11 and P12), and fast kinetics were also supported by the change in k_1 and $k_{1'}$ values (Table 2).

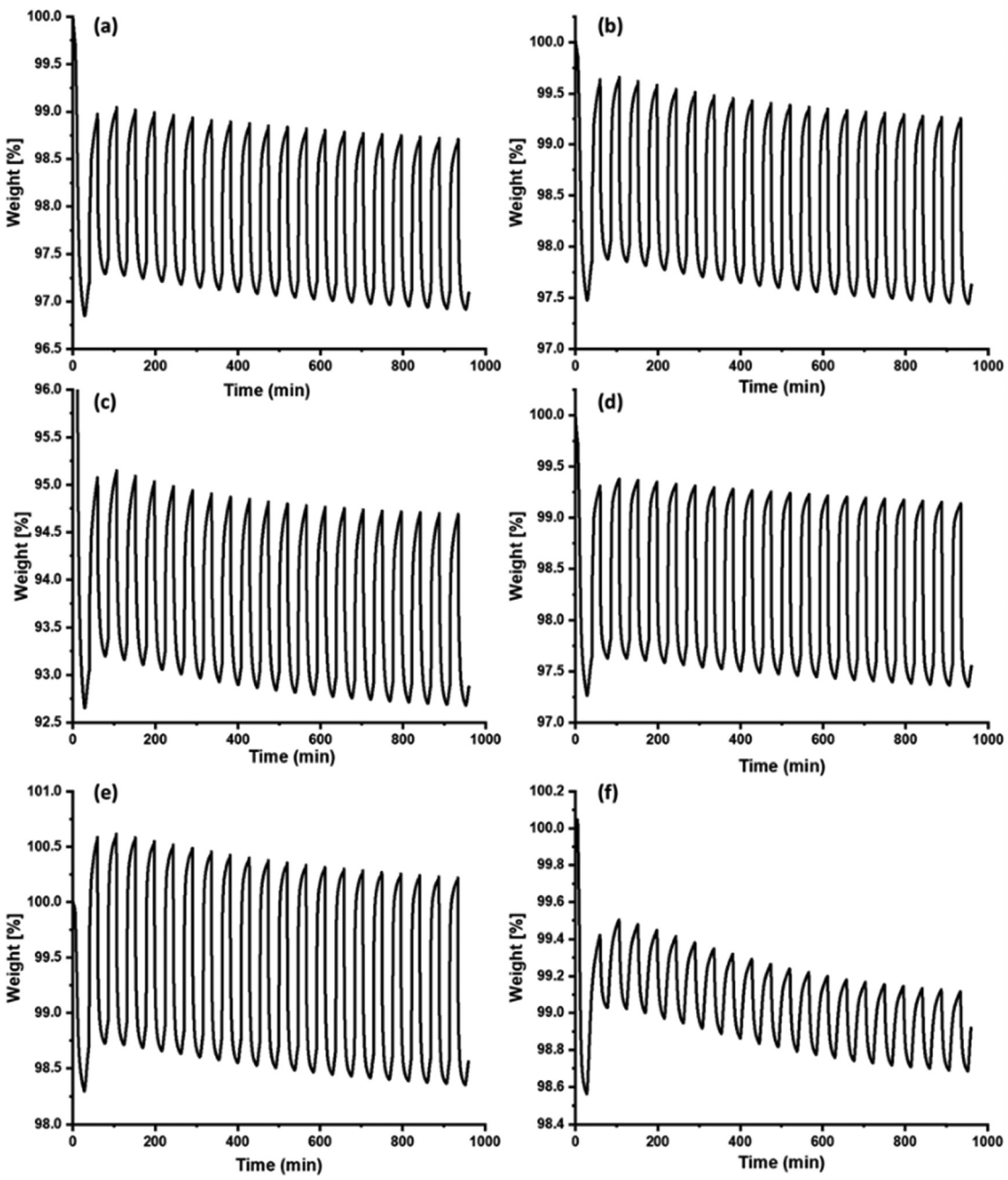

Fig. 5 20 cycles of CO_2 adsorption–desorption of porous carbon pellets. (a) P4, (b) P6, (c) P7, (d) P9, (e) P10. (f) Cyclic N_2 adsorption–desorption of the P7 pellet.

Similar trends were observed in the hollow cylindrical pellets (Fig. 3b). As the inner diameter increased (P14–P17), the overall CO_2 uptake increased. However, k_1 increased from 1.18 for P14 to 3.63 for P15 due to better diffusion of CO_2 (Table 2). Further changes in the diameter did not improve the kinetics, and the k_1 value became constant. P18, which is almost twice the size of other cylindrical hollow pellets (P15–P17), has a similar adsorption capacity to the other pellets. Then, a decrease in rate constant (k_1 and $k_{1'}$) suggested that a large inner diameter did not improve the kinetics further. This could be due to a decrease in contact time between the CO_2 and the surface, increasing the space velocity of CO_2, resulting in decreased kinetics. A powder sample was also used to determine the effects of binder and diffusion limitations in the pellets (Table 2 and Fig. S23 and S24, ESI†). Although, the pellets showed better performance compared to powder samples for both CO_2 uptake and k_1 (Table 2). $k_{1'}$ of the powder sample was found to be much higher than that of the pellets, which exhibited that CO_2 diffusion inside the pellets or carbon particles in the pellets is slower than that in the powder; however, the overall performance improved even better than the powder.

Effect of adsorption temperature and flow rate of CO_2

To further evaluate the pellets (P7), CO_2 adsorption isotherms were measured at three different temperatures (Fig. 4a, and Fig. S25, ESI†), and the effect of CO_2 flow rate was also analysed (Fig. 4b, and Fig. S26, ESI†). It is very well-known that the physical adsorption capacity significantly decreased at high temperature as the adsorption temperature increased from 25–75 °C. At 25 °C, P7 showed an adsorption capacity of 2.4 wt% within 15 min, which is still increasing and not yet saturated. At 50 °C and 75 °C, the adsorption capacity reduced to 1.3 wt% and 0.71 wt%, respectively, which showed that adsorption is completely physical. The pseudo-first-order model predicted an adsorption capacity that was quite close to the experimental adsorption capacity (Table 3).

The kinetic model showed the different k_1 and $k_{1'}$ values for all three adsorption temperatures, with a higher rate constant at 75 °C, indicating that the diffusion is faster at high temperatures despite a decrease in adsorption capacity (Table 3). P7 demonstrated maximum adsorption capacity at 25 °C, so the effect of CO_2 flow rate at a fixed adsorption temperature of 25 °C was measured and analysed. While the adsorption capacity did not change at different flow rates (Fig. 4b), both k_1 and $k_{1'}$ changed, with k_1 decreasing as the flow rate increased from 25 to 100 ml min^{-1} (Table 3). This indicates that higher molecular velocity reduces the contact time between the surface and CO_2 molecules. Apart from k_1 and $k_{1'}$, the total estimated adsorption capacity ($Q_{e1} + Q_{e2}$) was higher than the experimental data, which seems correct since none of the adsorption isotherms achieved saturation within 15 min.

Adsorption/adsorption cycles

Several pellets were investigated for cyclic CO_2 adsorption–desorption over 20 cycles (Fig. 5). All the pellets P4, P6, P7, P9, and P10 showed average CO_2 adsorption capacities of 1.8, 1.8, 2.0, 1.7, and 1.9 wt%, respectively, with no degradation in the CO_2 adsorption performance. The P7 pellets were also analysed for N_2 adsorption and found to be stable for 20 cycles under similar conditions. The pellet's N_2 adsorption capacity was 0.4 wt% (the powder sample also showed similar N_2 adsorption capacity), indicating that the pellets are not 100% selective for CO_2, typically a case of physical adsorption. The pellets exhibited selectivity of 79%, 79%, 88%, 75%, and 83% for P4, P6, P7, P9, and P10, respectively, for CO_2 over N_2 (assuming a constant N_2 adsorption capacity of 0.4 wt% for all pellets). However, a continuous mass loss could be due to the loss of physically adsorbed H_2O in the pore, and similar trends were even observed in powder samples (Fig. S27 and S28, ESI†). Low selectivity could be an issue in these pellets; however, they can be useful for CO_2 adsorption from other gas mixtures at reduced cost. Comparison with data published using physical adsorption of CO_2 are summarized in Table 4. The comparison showed that the pellet adsorption capacity is competitive compared to the powder samples. Most of the results in the

Table 4 Comparison with the reported CO_2 adsorption data using physical adsorption

Samples	Surface area (m^2 g^{-1})	Adsorption capacity (mmol g^{-1})	Selectivity	Shape	Ref.
Activated charcoal pellets	—	0.5 (at 30 °C, 1 atm, 15% CO_2)	70–90	Pellets	This work
Activated charcoal powder	850	0.4 (30 °C, 1 atm)	80	Powder	This work
Triamine grafted alumina pellet	84	0.46 (25 °C, 400 ppm)	—	Pellet	42
Triamine grafted silica pellet	395	0.38 (25 °C and 1 bar)	—	Pellets	51
MCM-48	1024	0.06 (50 °C and 1 atm)	—	Powder	59
Biochar	451	0.41 (120 °C and 1 atm) 1.77 (30 °C and 1 atm)	—	Powder	60
Activated fly ash	—	0.30 (30 °C and 1 atm)	—	Powder	61
Activated carbon bagasse	800	1.10 (25 °C and 1 bar)	—	Powder	62
Commercial activated carbon		0.25 (40 °C and 0.15 bar)	—	Powder	63
Carbon monolith	486	0.66 (30 °C, 100 kPa)	—	Powder	64
N-doped porous carbon	1770	4.40 (25 °C, 1 bar)	21	Powder	65
Porous carbon	762	2.36 (25 °C, and 1 bar)	18	Powder	66
Carbon fiber	2292	3.01 (25 °C, and 1 bar)	23	Fiber	67
MOF-based carbon monolith	516	0.76 1 (25 °C, and 1 bar)	10.6	Monolith	68
Microporous carbon monolith (NAC-800-3)	1154	2.81 (25 °C)	82.0	Monolith	69
Carbon monolith (CM950)	1225	1 (25 °C and 1 bar)	6.69	Monolith	70

literature were produced using power samples and volumetric adsorption of 100% CO_2.

Conclusions

As the shapes are changed to cylindrical (P8) and hollow cylindrical pellets (P9), the CO_2 uptake capacity is reduced compared to flakes (P7). The kinetic parameters differentiate the effect of two shapes (cylindrical and hollow cylindrical) (Table 1). The rate constant k_1 for P9, which was higher than P8, is likely due to the hollow nature of the pellets and thus better diffusion of CO_2 on the surface. However, it was lower than the k_1 value for the flake-like P7 (1.31) and the narrow cylinder P10 (1.41), reflecting the role of a larger exposed surface. As the size of the solid cylindrical pellets decreased, the CO_2 uptake capacity and kinetics parameters changed, indicating the high sensitivity of CO_2 adsorption to the size and shapes.

Compared to conventional powder sample analysis and reporting at the lab scale, designing and investigating pellets/monoliths/contractors under relevant industrial flue gas applications and direct air capture provided more reliable information and data to convert lab-scale invention to applied applications. Studying different sorbents in shaped forms advances fundamental investigation and understanding. We designed and investigated the physical adsorption of CO_2 in different sizes and shapes (spherical, solid cylindrical, hollow cylindrical, and flakes). Shaped pellets exhibited an average adsorption capacity of 0.5 mmol g^{-1} and were analysed for 20 cycles. However, the current pellets are not 100% selective for CO_2, and the pellets exhibited CO_2 selectivity of around 80% over N_2. This work can be seen as a reference to investigate and develop solid sorbents of different shapes and sizes for targeted applications. To further enhance the selectivity and adsorption capacity, chemical modification (surface hydrophobicity and compositing with silica, cellulose, *etc.*) of shaped pellets could be beneficial and advantageous for large-scale CO_2 capture.

Author contributions

B. S. Conceived ideas, design materials and experiments to record data and analysis, writing the original draft, review and editing, and project management. M. K. and B. S. SEM. imaging. T. R. Feedback, data discussion, and reviewing the final draft.

Data availability

The authors confirm that the data supporting the finding of this study are available within in the article and ESI.†

Conflicts of interest

The authors declare no competing financial interest.

Acknowledgements

BS and TR are grateful for financial support from Business Finland 8205/31/2022. SEM imaging was done in the ALD Centre Finland research infrastructure. We would like to thank Dr Risto Koivula for helping us with N_2 sorption analysis.

References

1 Daily CO_2 level, data my NOAA, **https://gml.noaa.gov/ccgg/trends/monthly.html**.
2 Z. Liu, Z. Deng, S. J. Davis and P. Ciais, *Nat. Rev. Earth Environ.*, 2024, **5**, 253–254.
3 S. Vaz, A. P. Rodrigues de Souza and B. E. Lobo Baeta, *Clean. Eng. Technol.*, 2022, **8**, 100456.
4 Y.-M. Wei, J.-N. Kang, L.-C. Liu, Q. Li, P.-T. Wang, J.-J. Hou, Q.-M. Liang, H. Liao, S.-F. Huang and B. Yu, *Nat. Clim. Change*, 2021, **11**, 112–118.
5 Y. Belmabkhout, V. Guillerm and M. Eddaoudi, *Chem. Eng. J.*, 2016, **296**, 386–397.
6 A. Rajendran, G. K. H. Shimizu and T. K. Woo, *Adv. Mater.*, 2024, **36**, 2301730.
7 R. Balasubramanian and S. Chowdhury, *J. Mater. Chem. A*, 2015, **3**, 21968–21989.
8 J. Y. Lai, L. H. Ngu and S. S. Hashim, *Greenhouse Gases: Sci. Technol.*, 2021, **11**, 1076–1117.
9 X. Wang, T. He, J. Hu and M. Liu, *Environ. Sci.: Nano*, 2021, **8**, 890–912.
10 M. Karimi, M. Shirzad, J. A. C. Silva and A. E. Rodrigues, *Environ. Chem. Lett.*, 2023, **21**, 2041–2084.
11 F. Raganati, F. Miccio and P. Ammendola, *Energy Fuel.*, 2021, **35**, 12845–12868.
12 A. A. Abd, S. Z. Naji, A. S. Hashim and M. R. Othman, *J. Environ. Chem. Eng.*, 2020, **8**, 104142.
13 R. Ben-Mansour, M. A. Habib, O. E. Bamidele, M. Basha, N. A. A. Qasem, A. Peedikakkal, T. Laoui and M. Ali, *Appl. Energy*, 2016, **161**, 225–255.
14 R.-S. Liu, X.-D. Shi, C.-T. Wang, Y.-Z. Gao, S. Xu, G.-P. Hao, S. Chen and A.-H. Lu, *ChemSusChem*, 2021, **14**, 1428–1471.
15 A. Sharma, J. Jindal, A. Mittal, K. Kumari, S. Maken and N. Kumar, *Environ. Chem. Lett.*, 2021, **19**, 875–910.
16 G. Singh, J. Lee, A. Karakoti, R. Bahadur, J. Yi, D. Zhao, K. AlBahily and A. Vinu, *Chem. Soc. Rev.*, 2020, **49**, 4360–4404.
17 B. Wen, Y. Li, C. Liang, Y. Chen, Y. Zhao and Q. Wang, *Langmuir*, 2024, **40**(16), 8327–8351.
18 Y. Shen, *Fuel Process. Technol.*, 2022, **236**, 107437.
19 M. S. Khosrowshahi, H. Mashhadimoslem, H. Shayesteh, G. Singh, E. Khakpour, X. Guan, M. Rahimi, F. Maleki, P. Kumar and A. Vinu, *Adv. Sci.*, 2023, **10**, 2304289.
20 D. G. Boer, J. Langerak and P. P. Pescarmona, *ACS Appl. Energy Mater.*, 2023, **6**, 2634–2656.
21 P. M. Bhatt, Y. Belmabkhout, A. Cadiau, K. Adil, O. Shekhah, A. Shkurenko, L. J. Barbour and M. Eddaoudi, *J. Am. Chem. Soc.*, 2016, **138**, 9301–9307.
22 K. Gopalsamy, D. Fan, S. Naskar, Y. Magnin and G. Maurin, *ACS Appl. Energy Mater.*, 2024, **2**, 96–103.

23 J.-B. Lin, T. T. T. Nguyen, R. Vaidhyanathan, J. Burner, J. M. Taylor, H. Durekova, F. Akhtar, R. K. Mah, O. Ghaffari-Nik, S. Marx, N. Fylstra, S. S. Iremonger, K. W. Dawson, P. Sarkar, P. Hovington, A. Rajendran, T. K. Woo and G. K. H. Shimizu, *Science*, 2021, **374**, 1464–1469.
24 S. S. Fatima, A. Borhan, M. Ayoub and N. Abd Ghani, *J. Mol. Liq.*, 2021, **338**, 116913.
25 H. J. Moon, R.-S. Sekiya and C. W. Jones, *J. Phys. Chem. C*, 2023, **127**, 11652–11665.
26 B. Singh and V. Polshettiwar, *Pure Appl. Chem.*, 2023, **95**, 451–462.
27 B. Singh, J. Na, M. Konarova, T. Wakihara, Y. Yamauchi, C. Salomon and M. B. Gawande, *Bull. Chem. Soc. Jpn.*, 2020, **93**, 1459–1496.
28 B. Singh and V. Polshettiwar, *Nanoscale*, 2019, **11**, 5365–5376.
29 B. Singh and V. Polshettiwar, *J. Mater. Chem. A*, 2016, **4**, 7005–7019.
30 M. Bisht Bhawna, B. Singh and S. Pandey, *J. Mol. Liq.*, 2023, **384**, 122203.
31 A. Hakim, T. S. Marliza, N. M. Abu Tahari, R. W. N. Wan Isahak, R. M. Yusop, W. M. Mohamed Hisham and A. M. Yarmo, *Ind. Eng. Chem. Res.*, 2016, **55**, 7888–7897.
32 Z. Zhang, Z. P. Cano, D. Luo, H. Dou, A. Yu and Z. Chen, *J. Mater. Chem. A*, 2019, **7**, 20985–21003.
33 M. Oschatz and M. Antonietti, *Energy Environ. Sci.*, 2018, **11**, 57–70.
34 W. Gao, S. Liang, R. Wang, Q. Jiang, Y. Zhang, Q. Zheng, B. Xie, C. Y. Toe, X. Zhu, J. Wang, L. Huang, Y. Gao, Z. Wang, C. Jo, Q. Wang, L. Wang, Y. Liu, B. Louis, J. Scott, A.-C. Roger, R. Amal, H. He and S.-E. Park, *Chem. Soc. Rev.*, 2020, **49**, 8584–8686.
35 B. Singh, A. Maity and V. Polshettiwar, *ChemistrySelect*, 2018, **3**, 10684–10688.
36 A. Kaithwas, M. Prasad, A. Kulshreshtha and S. Verma, *Chem. Eng. Res. Des.*, 2012, **90**, 1632–1641.
37 Q. Wang, J. Luo, Z. Zhong and A. Borgna, *Energy Environ. Sci.*, 2011, **4**, 42–55.
38 M. Khraisheh, F. Almomani and G. Walker, *Sci. Rep.*, 2020, **10**, 269.
39 B. Singh, Z. E. Gorgi, R. Singh and V. Sharma, Timo Repo, Silica Gel Supported Solid Amine Sorbent for CO_2 Capture, *Energy Environ. Mater.*, 2024, 200.
40 B. Verougstraete, A. Martín-Calvo, S. Van der Perre, G. Baron, V. Finsy and J. F. M. Denayer, *Chem. Eng. J.*, 2020, **383**, 123075.
41 L. Jiang, W. Liu, R. Q. Wang, A. Gonzalez-Diaz, M. F. Rojas-Michaga, S. Michailos, M. Pourkashanian, X. J. Zhang and C. Font-Palma, *Prog. Energy Combust. Sci.*, 2023, **95**, 101069.
42 Q. Grossmann, V. Stampi-Bombelli, A. Yakimov, S. Docherty, C. Copéret and M. Mazzotti, *Ind. Eng. Chem. Res.*, 2023, **62**, 13594–13611.
43 F. Hussin, N. Nadira Hazani and M. Kheireddine Aroua, *Mater. Today: Proc.*, 2023, DOI: **10.1016/j.matpr.2023.01.094**.
44 Q. Hu, J. Shao, H. Yang, D. Yao, X. Wang and H. Chen, *Appl. Energy*, 2015, **157**, 508–516.
45 X. Zhu, W. Xie, J. Wu, Y. Miao, C. Xiang, C. Chen, B. Ge, Z. Gan, F. Yang, M. Zhang, D. O'Hare, J. Li, T. Ge and R. Wang, *Chem. Soc. Rev.*, 2022, **51**, 6574–6651.
46 L. Estevez, D. Barpaga, J. Zheng, S. Sabale, R. L. Patel, J.-G. Zhang, B. P. McGrail and R. K. Motkuri, *Ind. Eng. Chem. Res.*, 2018, **57**, 1262–1268.
47 R. Wang, P. Wang, X. Yan, J. Lang, C. Peng and Q. Xue, *ACS Appl. Mater. Interfaces*, 2012, **4**, 5800–5806.
48 M. Sevilla, J. B. Parra and A. B. Fuertes, *ACS Appl. Mater. Interfaces*, 2013, **5**, 6360–6368.
49 M. Sevilla and A. B. Fuertes, *Energy Environ. Sci.*, 2011, **4**, 1765–1771.
50 R. Wang, S.-C. Xi, D.-Y. Wang, M. Dou and B. Dong, *ACS Appl. Nano Mater.*, 2021, **4**, 10148–10154.
51 B. Wadi, A. Mahomed, Y. Bai, A. Osatiashtiani, V. Manovic and S. A. Nabavi, *Powder Technol.*, 2021, **393**, 257–264.
52 F. Rezaei, M. A. Sakwa-Novak, S. Bali, D. M. Duncanson and C. W. Jones, *Microporous Mesoporous Mater.*, 2015, **204**, 34–42.
53 Y. R. Dangi, J. K. Bediako, X. Lin, J.-W. Choi, C.-R. Lim, M.-H. Song, M. Han and Y.-S. Yun, *Sci. Rep.*, 2021, **11**, 17836.
54 B. Singh, M. Kemell, J. Yliniemi and T. Repo, *Nanoscale*, 2024, **16**, 16251–16259.
55 V. K. Singh and E. A. Kumar, *Greenhouse Gases: Sci. Technol.*, 2017, **7**, 182–201.
56 S. Yang, L. Peng, O. A. Syzgantseva, O. Trukhina, I. Kochetygov, A. Justin, D. T. Sun, H. Abedini, M. A. Syzgantseva, E. Oveisi, G. Lu and W. L. Queen, *J. Am. Chem. Soc.*, 2020, **142**, 13415–13425.
57 F. Raganati, M. Alfe, V. Gargiulo, R. Chirone and P. Ammendola, *Chem. Eng. J.*, 2019, **372**, 526–535.
58 N. Querejeta, F. Rubiera and C. Pevida, *ACS Sustainable Chem. Eng.*, 2022, **10**, 2107–2124.
59 H. T. Jang, Y. Park, Y. S. Ko, J. Y. Lee and B. Margandan, *Int. J. Greenhouse Gas Control*, 2009, **3**, 545–549.
60 X. Zhang, S. Zhang, H. Yang, J. Shao, Y. Chen, Y. Feng, X. Wang and H. Chen, *Energy*, 2015, **91**, 903–910.
61 C. Siriruang, P. Toochinda, P. Julnipitawong and S. Tangtermsirikul, *J. Environ. Manag.*, 2016, **170**, 70–78.
62 M. Alhassan, I. Andrew, M. Auta, M. Umaru, M. U. Garba, A. G. Isah and B. Alhassan, *Biofuels*, 2018, **9**, 719–728.
63 P. Ammendola, F. Raganati and R. Chirone, *Chem. Eng. J.*, 2017, **322**, 302–313.
64 S. Hosseini, E. Marahel, I. Bayesti, A. Abbasi, L. Chuah Abdullah and T. S. Y. Choong, *Appl. Surf. Sci.*, 2015, **324**, 569–575.
65 J. Shao, J. Wang, Q. Yu, F. Yang, M. Demir, O. C. Altinci, A. Umay, L. Wang and X. Hu, *Sep. Purif. Technol.*, 2024, **333**, 125891.
66 T. Lu, J. Bai, J. Huang, Q. Yu, M. Demir, M. Kilic, B. N. Altay, L. Wang and X. Hu, *Energy Fuel*, 2023, **37**, 3886–3893.
67 C. Ma, T. Lu, M. Demir, Q. Yu, X. Hu, W. Jiang and L. Wang, *ACS Appl. Nano Mater.*, 2022, **5**, 13473–13481.
68 D. Qian, C. Lei, G.-P. Hao, W.-C. Li and A.-H. Lu, *ACS Appl. Mater. Interfaces*, 2012, **4**, 6125–6132.
69 Z. Geng, Q. Xiao, H. Lv, B. Li, H. Wu, Y. Lu and C. Zhang, *Sci. Rep.*, 2016, **6**, 30049.
70 J. Singh, H. Bhunia and S. Basu, *J. Taiwan Inst. Chem. Eng.*, 2018, **89**, 140–150.